Stator Interturn Fault Detection of Synchronous Machines Using Field Current and Rotor Search-Coil Voltage Signature Analysis

Prabhakar Neti, *Member, IEEE*, and Subhasis Nandi, *Senior Member, IEEE*

***Abstract*—Our recent observations suggested that harmonics in the field current are very promising to detect stator interturn faults in synchronous machines. So far, an increase in some of the even harmonics in the field current has been reported to detect such faults. However, no explanation has been provided for the cause of these harmonics. Moreover, the even harmonics can significantly increase with supply unbalance as well as time harmonics, which can lead to a serious confusion. Hence, in this study, an in-depth investigation was conducted to determine the origin of various harmonic components in the field current and their feasibility to detect stator faults. It was found that, owing to structural asymmetries of the field winding, some of these components clearly increased with stator interturn fault. The findings are helpful to detect faults involving few turns without ambiguity, in spite of the presence of supply unbalance and time harmonics. Both simulation and experimental results are presented in this paper. The diagnosis results have also been verified using a rotor-mounted search coil, which can also be used to detect even a one-turn stator fault very effectively.**

***Index Terms*—Interturn fault, modified winding function approach (MWFA), synchronous motor, winding function approach (WFA).**

I. Introduction

THE LOSS of the dielectric strength of the winding insulation in electric machines leads to interturn faults. The time elapsed in the growth of an incipient fault leading to a catastrophic failure of the machine varies from a third of a second to several minutes in the case of random-wound machines and can even be much longer in the case of form-wound machines [1]. Hence, an early detection of such faults involving few turns is very much desirable in order to protect them. Several researchers have attempted to detect interturn faults in the field circuit [2]–[4]. An attempt has also been made to analyze the transient behavior of salient-pole synchronous machines with internal stator winding faults [5].

Paper IPCSD-08-078, presented at the 2006 Industry Applications Society Annual Meeting, Tampa, FL, October 8–12, and approved for publication in the IEEE TRANSACTIONS ON INDUSTRY APPLICATIONS by the Electric Machines Committee of the IEEE Industry Applications Society. Manuscript submitted for review April 1, 2007 and released for publication October 19, 2008. Current version published May 20, 2009. This work was supported in part by the Natural Sciences and Engineering research Council of Canada, in part by CFI, and in part by Uvic.

P. Netri is with the Electric Machines and Drives Laboratory, Electronics and Energy Conversion, General Electric Global Research Center, Niskayuna, NY USA 12309 (e-mail: netipr@ge.com).

S. Nandi is with the Department of Electrical and Computer Engineering, University of Victoria, Victoria, BC V8W 3P6, Canada (e-mail: snandi@ece.uvic.ca).

Digital Object Identifier 10.1109/TIA.2009.2018905

Many researchers have analyzed the field current of synchronous machines against stator and rotor interturn faults [6]–[8]. Particularly, an increase of the eighth harmonic in the field current of a four-pole synchronous generator with a stator fault was highlighted in [6]. A detailed analysis has been presented on brushless synchronous generators using the 180-Hz positive-sequence stator voltage as an indicator of stator fault, the 30-, 90-, and 150-Hz armature circulating currents as indicators of field winding deterioration, and the 120-Hz exciter field current as an indicator of rotating rectifier diode shorts [7].

As discussed later in this paper, some of the even harmonics in the field current (including the eighth harmonic) can increase with supply unbalance and time harmonics that can lead to a serious confusion. Hence, in order to detect stator interturn faults in salient-pole synchronous motors unambiguously, some of the other frequency components in the field current have been monitored. It was observed that, owing to the structural asymmetries of the field winding, a stator interturn fault could increase these components in the field current. The frequency components that showed a clear increase due to stator faults but were least affected by the supply unbalance and time harmonics have been highlighted. The internal asymmetry of the machine, which affected earlier diagnosis results adversely, has now been used to an advantage for the first time. Hence, the unambiguous detection of interturn faults was possible with high sensitivity. A detailed mathematical analysis of this phenomenon has also been presented.

In practice, all the machines are expected to possess internal asymmetries due to the manufacturing imperfections and nonhomogeneity of iron. The asymmetries can be in the magnetic path, stator winding, air gap, and/or rotor cage/winding. In the present study, simulation results have been obtained by introducing asymmetry in the field winding. Experimental results have been obtained by physically shorting different numbers of stator turns in a 2-kW motor. A comparative study of the characteristic frequency components has been put forward with different fault levels and supply unbalance. The influence of the load and power factor (PF) of the machine on the test results is also discussed. The test results have also been verified by performing a harmonic analysis on the voltage induced in a rotor-mounted search coil, which can also be used for stator fault detection very effectively, *even up to one shorted turn*. The additional cost of installing a search coil may be customized to those customers who would need a high-sensitivity fault detection scheme. However, a field-current-based monitoring

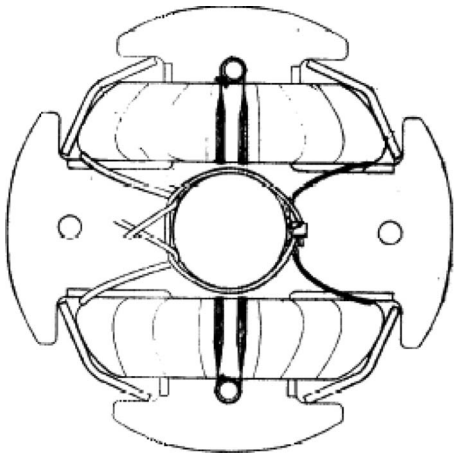

Fig. 1. Rotor cross section of synchronous motor with a two-coil field winding.

is always possible without any modification. The proposed method can be used for both salient-pole and round-rotor synchronous machines.

In order to protect the motor using the proposed scheme, only one signal needs to be monitored. Hence, it is very easy to implement this scheme compared with the negative-sequence technique [1] that requires at least four sensors (two for line voltages and two for line currents). Less number of sensors implies less number of channels of the data acquisition system, less data processing, and therefore, a very high-speed tripping of the faulty machine at a lower cost. Furthermore, in a recent study, it has been found that the negative-sequence-based detection can cause very serious ambiguity, particularly to detect faults involving very few shorted turns in the stator winding [9]. Ambiguity arises due to the fact that supply unbalance can change the sequence impedances in the machine, and hence, the accurate prediction of the negative-sequence current component due to supply unbalance and internal asymmetry is nearly impossible.

II. Description of Motor and Selection of Fault

The salient-pole synchronous motor under consideration is a 208-V 1800-r/min 60-Hz 2-kW four-pole random-wound machine having 36 stator slots. The stator has a three-phase double-layer lap winding, and the rotor has 20 damper bars. The field winding of the machine is composed of two series-connected coils, each placed on the diagonally opposite rotor poles. This has been done for the *ease of construction*. Each coil side occupies each of the interpolar gaps. The cross section of the rotor of the synchronous motor with a two-coil field winding is shown in Fig. 1. A search coil is also mounted on one of the pole faces of the rotor. Furthermore, several taps have been brought out from the stator winding (phase-a) to physically create the interturn faults.

Ideally, although the flux pattern produced by *the two-coil field winding* will be similar to that produced by a *standard four-coil field winding* (one coil on each pole), their turn functions are different as given later in (9) and (10). However, due to the inevitable manufacturing and magnetic asymmetries, the turn function of any actual field winding will be more like the one given in (11). This will be referred to as the *asymmetric field winding*.

III. Mechanism of Induction of Even Harmonics in Field Current Under Supply Unbalance

With unbalanced three-phase voltages, a balanced three-phase stator winding produces a reverse-rotating MMF wave [in ampere-turns (AT)] given as

$$F_s = A_s \cos[np\phi \pm \omega t]. \tag{1}$$

$n = (6k \pm 1)$, other than fundamental, is the order of space harmonics produced by a balanced three-phase stator winding, $k = 1, 2, 3, \ldots$, ϕ is the angular position with respect to the stator, p is the number of fundamental pole pairs, $\omega = 2\pi f$, and f is the supply frequency. Considering only the dc part (P_0) of the specific permeance function (in Wb/AT $\cdot$ m^2) [10], the flux density (in teslas) produced by this MMF, with respect to the stator, can be given as

$$B_s = A_s P_0 \cos(np\phi \pm \omega t) \tag{2}$$

or with respect to the rotor

$$B_r = A_s P_0 \cos(np\phi' + np\omega_s t \pm \omega t + \varphi_1). \tag{3}$$

Here, ϕ' is the angular position with respect to the rotor, and ω_s is the synchronous speed in radians per second. Substituting $\omega_s = \omega/p$ in (3), the flux density with respect to the rotor, can be given as

$$B_r = A_s P_0 \cos\{np\phi' + (n \pm 1)\omega t + \varphi_1\}. \tag{4}$$

B_r can induce a particular frequency component in a winding if and only if the pole pair of B_r corresponding to that frequency matches with one of the pole pairs of the winding [11]. From (4), the 120-Hz component is produced with $n = 1$, a "+" sign before 1, and $f = 60$ Hz. The pole pair associated with the 120-Hz component is $n^*p = 2$ for the chosen motor. Hence, the 120-Hz component can be induced in the two-coil, four-coil, and asymmetric field windings, since all of these windings can produce the pole-pair number 2 as seen in (9)–(11). For $n = 5$ and a "$-$" sign before 1, the 240-Hz component can be produced. Similarly, due to supply unbalance, other even harmonics (including the eighth harmonic) can be induced in the two-coil, four-coil, and *asymmetric* windings whose turn functions are given in (9)–(11). Clearly, since the eighth harmonics were used for fault detection in [6], ambiguous detection is very likely.

IV. Mechanism of Induction of Various Harmonic Components in Field Current With Stator Fault

In the case of a synchronous motor with stator interturn faults, the induction of various harmonic components in the field winding can be proved as follows. The stator has a shorted loop (can thus be treated as a single-phase winding) carrying

TABLE I
HARMONIC COMPONENTS IN FIELD CURRENT

k	1	2	3	4	5	6	7	8	9	10
Freq. (Hz)	30	0	30	60	90	120	150	180	210	240
	90	120	150	180	210	240	270	300	330	360

current at a supply frequency that generates two counterrotating MMF waves [12], which can be given as

$$F_{sf} = A_f \cos[k\phi \pm \omega t] \tag{5}$$

where $k = 1, 2, 3, \ldots$. Considering the dc part of the specific permeance function (P_0), the flux density produced by this MMF, with respect to the stator, can be given as

$$B_{sf} = A_f P_0 \cos(k\phi \pm \omega t) \tag{6}$$

or with respect to the rotor

$$B_{rf} = A_f P_0 \cos(k\phi' + k\omega_s t \pm \omega t + \varphi_2). \tag{7}$$

Substituting $\omega_s = \omega/p$ in (7), we can have

$$B_{rf} = A_f P_0 \cos\left[k\phi' + \{(k/p) \pm 1\}\,\omega t + \varphi_2\right]. \tag{8}$$

The components that showed promise from experiments are 60, 90, 150, and 210 Hz. With $p = 2$ and $k = 4$, from (8), the 60-Hz component can be produced. Since $k = 4$, the 60-Hz component can be induced in the symmetric winding of a two-coil structure and the *asymmetric* windings of both structures, since the *asymmetric* winding can produce all $k = 1, 2, 3$, etc., pole pairs, as given in (11). However, its magnitude is expected to be much higher for the two-coil structure since the pole-pair number 4 arises out of the symmetric structure itself. Similarly, with $k = 1$, 3, 5, and 7, the 90- and 150-Hz components can be induced in the *asymmetric* field winding. These components cannot be induced in the ideal two- and four-coil field windings, since these windings produce pole-pair numbers 2, 4, 6, etc., (9) and 2, 6, 10, etc., (10), respectively. Using a similar argument, it can be shown that all other even harmonics (120, 240, 360, 480 Hz, etc.) can also be induced in the ideal two-coil, four-coil, as well as *asymmetric* field windings due to an interturn fault in the stator winding. Table I shows, for different values of "k" and $p = 2$, the various harmonics that can be induced in the asymmetric field winding with a 60-Hz utility supply.

Furthermore, this method can be used for a synchronous machine having any pole-pair number. The frequency component that is sensitive to an interturn fault has to be chosen based on the pole-pair number of the machine. As an example, in the case of a two-pole machine, i.e., $p = 1$, the fault detector components in the field current or the rotor search-coil voltage can be calculated as 60, 180 Hz, etc., from (8). The components induced by the supply unbalance following (4) are only even harmonics (120, 240, 480 Hz, etc.) of the fundamental and, therefore, will not affect detection.

V. MODELING OF SYNCHRONOUS MOTOR WITH STATOR INTERTURN FAULT AND ASYMMETRIC FIELD WINDING

In order to carry out the simulation studies, the salient-pole synchronous motor has been modeled including the damper bars. The following are the four different machine models obtained for each of the two-coil and the four-coil field windings: 1) *healthy* machine with *symmetric* field winding; 2) *healthy* machine with *asymmetric* field winding; 3) *faulty* machine with *symmetric* field winding; and 4) *faulty* machine with *asymmetric* field winding. Thus, a total of *eight* different models were obtained. The asymmetric field winding has been modeled by choosing a different number of turns in one of the coils. The models of faulty machines can accommodate different numbers of shorted turns in the stator winding.

In order to develop a model of a synchronous machine, various magnetizing and mutual inductances of the machine are to be computed for different rotor positions. These inductances can be computed using the winding function approach (WFA) and the modified WFA (MWFA) [13]–[16]. WFA and MWFA consider the physical distribution of various windings in the machine represented by their turn functions. The Fourier series expansions of the turn functions of the *symmetric* two-coil and standard field windings are expressed in (9) and (10), respectively. The Fourier series expansion given in (11) represents the general form of *asymmetric* field windings. The coefficients will be different for the two-coil and standard structures. "θ_d" and "θ_q" are the angles subtended by the rotor polar and interpolar arcs at the center, respectively. Using (9), the turn function of a *symmetric* two-coil field winding has been plotted as shown in Fig. 2 (top). Similarly, using (10), the turn function of a *symmetric* standard field winding has been plotted as shown in Fig. 3 (top). Asymmetry can be introduced in the field winding by removing a few turns from one of the coils of the winding. The turn functions of the *asymmetric* two-coil and standard structures have been shown in the bottom plots of Figs. 2 and 3, respectively,

$$n_{rf1}(\phi,\theta) = a_{orf1} + \sum_{m=1,2,3,\ldots}^{\infty} a_{mrf1} \cos\left[pm(\phi-\theta)\right] \tag{9}$$

$$a_{orf1} = \frac{N_{rf}\theta_d}{\pi};\ N_{rf} = 1260;\ a_{mrf1} = \frac{2N_{rf}}{\pi m}\sin(m\theta_d)$$

$$n_{rf2}(\phi,\theta) = a_{orf2} + \sum_{q=1,3,5,\ldots}^{\infty} a_{qrf2} \cos\left[pq(\phi-\theta)\right] \tag{10}$$

$$a_{orf2} = \frac{N_{rf}}{2};\ N_{rf} = 1260;\ a_{qrf2} = \frac{2N_{rf}}{\pi q}\sin(q\theta_d)$$

$$n_{rfa}(\phi,\theta) = a_{orfa} + \sum_{w=1,2,3,\ldots}^{\infty} a_{wrfa} \cos\left[w(\phi-\theta)\right]. \tag{11}$$

After computing various magnetizing and mutual inductances of the machine using WFA and MWFA [13]–[16], the dynamic models of the synchronous motor have been obtained using the coupled circuit approach [15]. The mutual inductances between stator phase-a and the field windings with both the symmetric and asymmetric cases are shown in Fig. 4

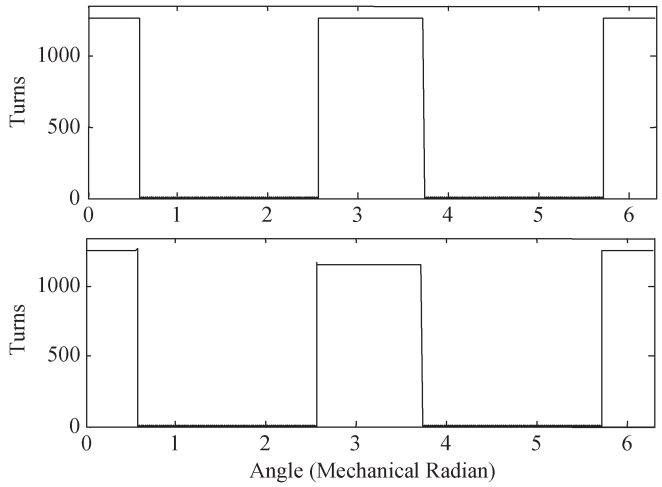

Fig. 2. Turn functions of the two-coil field winding, (top) symmetric and (bottom) asymmetric.

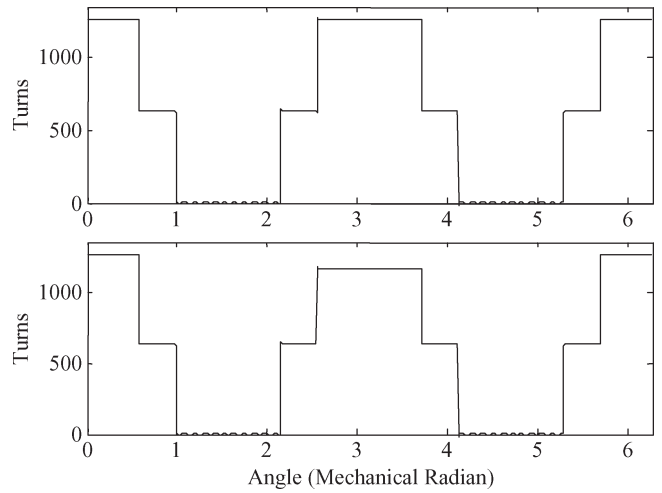

Fig. 3. Turn functions of the standard field winding, (top) symmetric and (bottom) asymmetric.

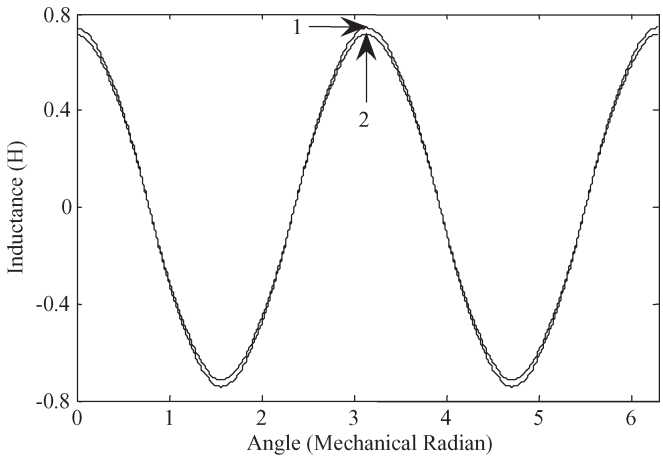

Fig. 4. Mutual inductance between the stator phase-a and two-coil field windings, (1) symmetric and (2) asymmetric.

(for two-coil structure) and Fig. 5 (for standard structure). In a similar manner, an interturn fault in the stator winding can be simulated [17] as elaborated in the Appendix.

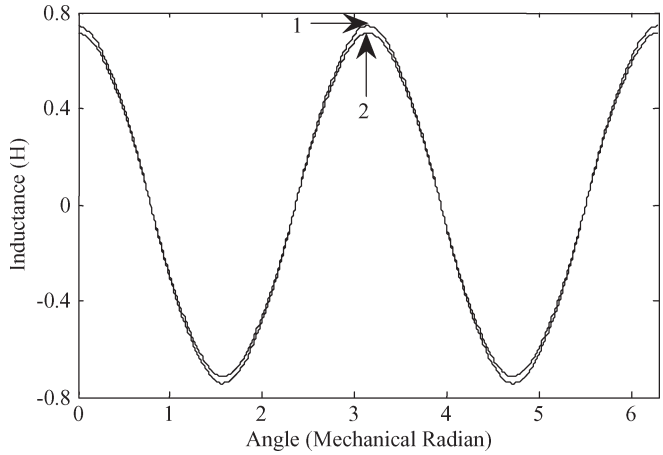

Fig. 5. Mutual inductance between the stator phase-a and standard field windings, (1) symmetric and (2) asymmetric.

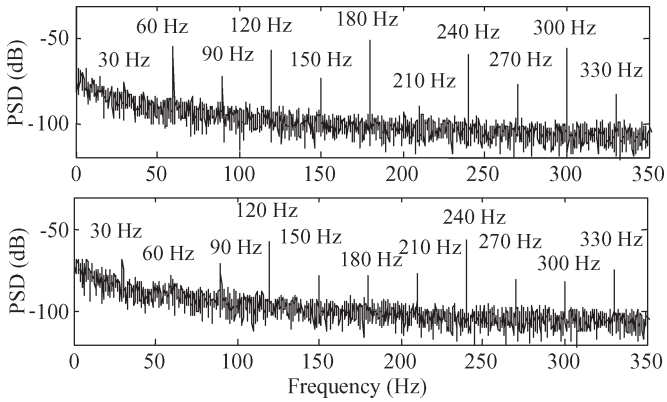

Fig. 6. Power spectral density (PSD) of field current of the simulated motor with (top) asymmetric two-coil and (bottom) standard field winding with four-turn fault.

VI. Simulation Results

A thorough simulation study was carried out using the eight different models of the machine as mentioned in the earlier section. The results were obtained at full-load, 0.88 lagging PF and rated field current of the machine. The spectra for the motor models with asymmetric two- and four-coil field windings and four-turn fault are shown in Fig. 6. Since the coefficients of the cosine functions in (11) are different for the two structures, the frequency components in the two have dissimilar magnitudes. However, *no components other than those predicted by* Table I *show up, conclusively proving the theory presented in* Section IV. A detailed comparative study of the various frequency components in the field current has also been presented, as shown in Figs. 7 and 8. The condition of the motor is shown on the x-axis of the plots. "HB" and "HU" denote the healthy machine fed by balanced and unbalanced supplies, respectively, whereas "T1" to "T4" represent one to four shorted turns in the stator winding. The plots have been normalized with respect to the dc component of the field current. As predicted in the preceding sections, the 120- and 480-Hz components showed up with supply unbalance as well as with turn faults. This was observed in the case of the symmetric and asymmetric field windings of both structures. Hence, the

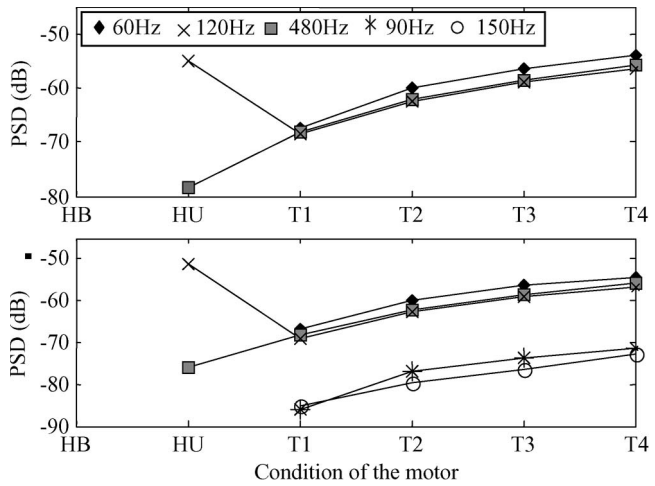

Fig. 7. Frequency components in the field current of the simulated motor with a two-coil structure, (top) symmetric and (bottom) asymmetric.

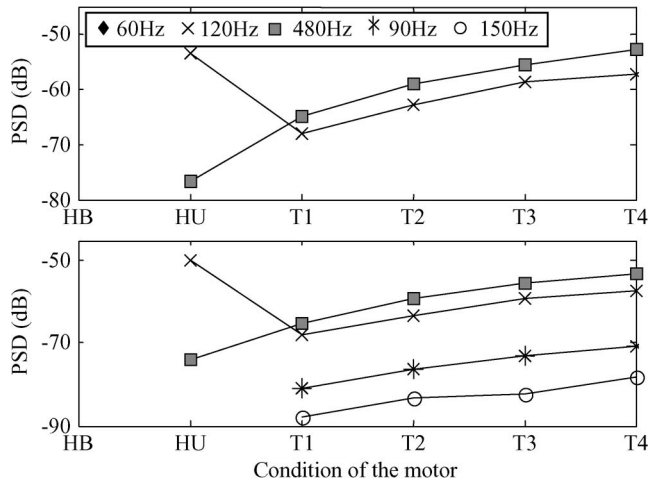

Fig. 8. Frequency components in the field current of the simulated motor with standard structure, (top) symmetric and (bottom) asymmetric.

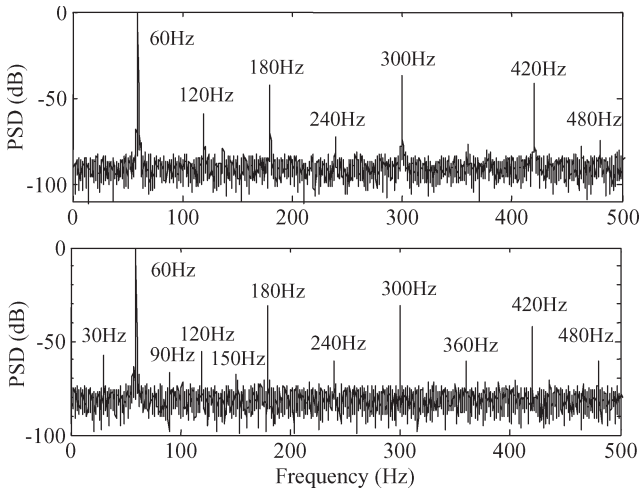

Fig. 9. PSD of the (top) line voltage and (bottom) line current of the experimental motor with two-coil field winding.

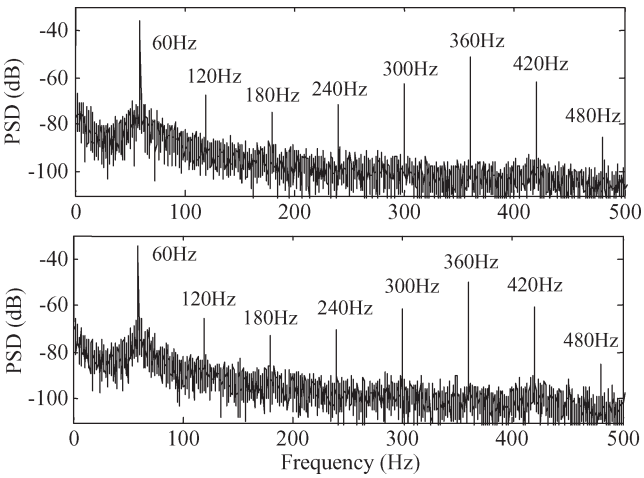

Fig. 10. PSD of the field current of the simulated motor with (top) asymmetric two-coil and (bottom) standard field windings with utility voltage data.

changes in the even harmonics may not clearly distinguish the faulty and unbalanced supply conditions.

In the case of both the symmetric and asymmetric two-coil structures of the field winding, the 60-Hz components were sensitive to the interturn faults as predicted. However, these components did not show any increase in the symmetric standard field winding as predicted and did not increase significantly even in the case of the asymmetric winding for the chosen amount of asymmetry.

Most importantly, in the case of the asymmetric windings of both structures, the 90- and 150-Hz components showed a clear increase *only* with stator faults as predicted. Furthermore, in the case of the healthy machine with both symmetric and asymmetric field windings, these components were absent with supply unbalance as shown in Figs. 7 and 8.

The utility supply has many time harmonics, which can also induce some harmonic components in the field current. In order to investigate their influence, first, the spectra of the line voltage and the line current of the experimental motor (with two-coil structure) are obtained, as shown in Fig. 9. It is interesting to note that the line current has more harmonics than the voltage, such as 30, 90, 150 Hz, etc. It is therefore very clear that these additional harmonics are due to causes internal to the machine. Some of these causes are eccentricity, saturation, structural asymmetry, etc. All these frequency components can induce various harmonics in the field current of an actual machine, as can be seen from Figs. 11 and 15 in Section VII. However, with the kind of asymmetry considered for simulation, only supply voltage harmonics are reflected back in the field current (Fig. 10) and not the 30-, 90-, and 150-Hz components. Fig. 10 has been obtained using the actual voltage data collected from the utility supply.

VII. Experimental Results

A motor that has a two-coil field winding was rigorously tested in the laboratory with different fault levels at various loads and PFs. In order to ensure the unambiguous detection of the fault, the influence of supply unbalance on the test results was also carefully observed.

The synchronous machine under test is coupled to a dc generator. The dc generator is loaded with a resistance bank.

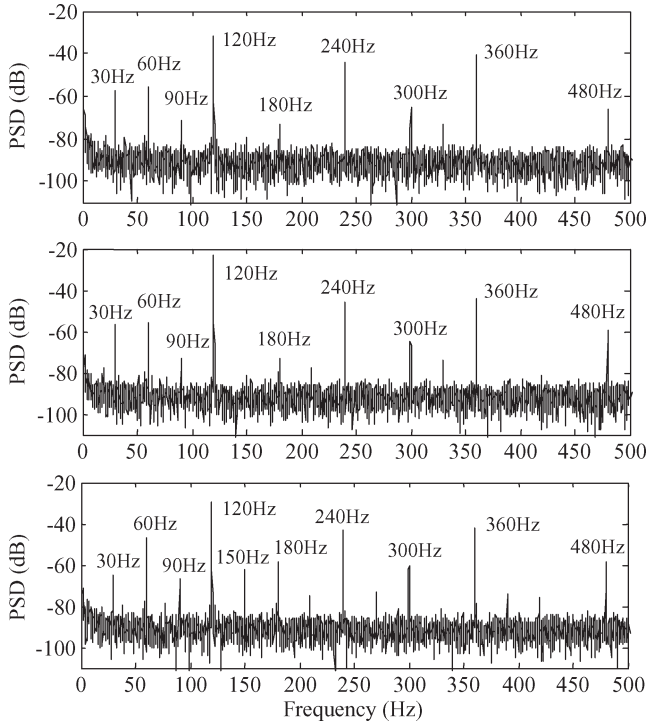

Fig. 11. Experimental PSD of field current under full-load, 0.8 lagging PF condition (top) with balanced supply, (middle) with unbalanced supply, and (bottom) with four-turn fault for the two-coil field winding.

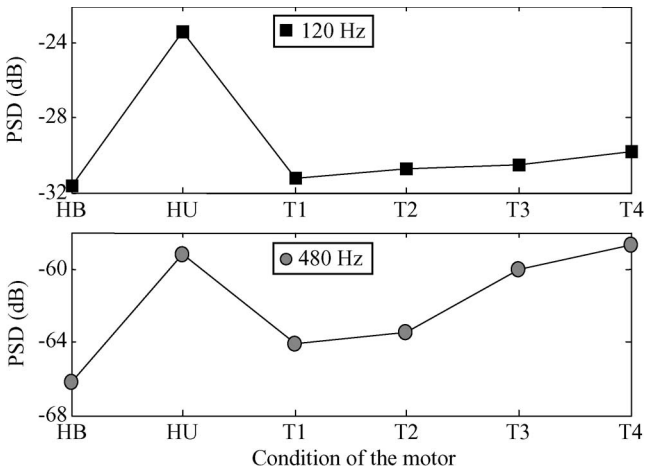

Fig. 12. (Top) 120- and (bottom) 480-Hz components in the field current under full-load 0.8 lagging PF condition (experimental).

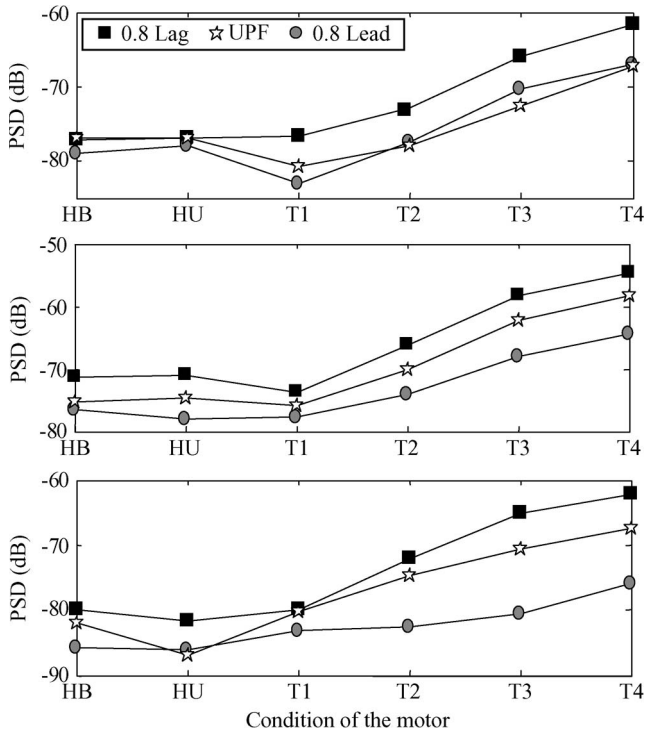

Fig. 13. 150-Hz component in the field current under (top) no-load, (middle) half-load, and (bottom) full-load (experimental).

An interturn fault is created in the stator winding of the synchronous machine with the help of a timer-controlled contactor. The timer helps to automatically clear the fault after a preset time to ensure safety during testing. The field current is monitored with the help of a Hall-effect current sensor. The search-coil voltage is monitored using a voltage probe. The data are collected using a data acquisition system. Since the tests with interturn faults were conducted for many times, a sufficient time gap is allowed between consecutive interturn short circuit tests to cool down the machine and not to stress the machine insulation.

It was also noticed that the sensitivity of the current sensor is vitally important in detecting the harmonics in question. Otherwise, they may get lost in the noise floor. A Hall-effect current sensor was used to measure the field current which has an attenuation factor of 1/10. In order to increase the sensitivity, six more turns are used for the current sensor which brought down the attenuation factor to 6/10. Further amplification was not possible as the dc component of the field current saturated the existing current probe.

A significant increase in the 120- and 480-Hz harmonics was observed in the field current of the healthy machine with supply unbalance ($V_{\rm ab} = 199.9$ V, $V_{\rm bc} = 208.1$ V, and $V_{\rm ca} = 206.9$ V), as shown in Fig. 11. The variation of the 120- and 480-Hz harmonics under supply unbalance and turn-fault condition of the motor at full-load (0.8 lag) is shown in Fig. 12. An even larger increase of these harmonics under supply unbalance compared with faulty conditions clearly indicates the *ambiguity*.

The 150-Hz components in the excitation current showed the most prominent increase with the faults involving a few turns. This was observed at all the three PFs under no-load, half-load, and full-load conditions, as shown in Fig. 13. The supply unbalance seems to have minimal influence on this harmonic.

Furthermore, the harmonic analysis of the voltage induced in the rotor-mounted search coil showed an even more encouraging increase of these frequency components with stator interturn fault. The rotor search coil can accept a frequency of any pole-pair number *independent* of the asymmetry in the machine. The 90-Hz component in the rotor search-coil voltage was found to be a *very promising* indicator of even a *one-turn* fault at all operating conditions and was least affected by supply unbalance, as shown in Fig. 14. The magnitudes of different harmonics have been normalized with respect to the dc and the 30-Hz components of the field current and the rotor search-coil voltage, respectively.

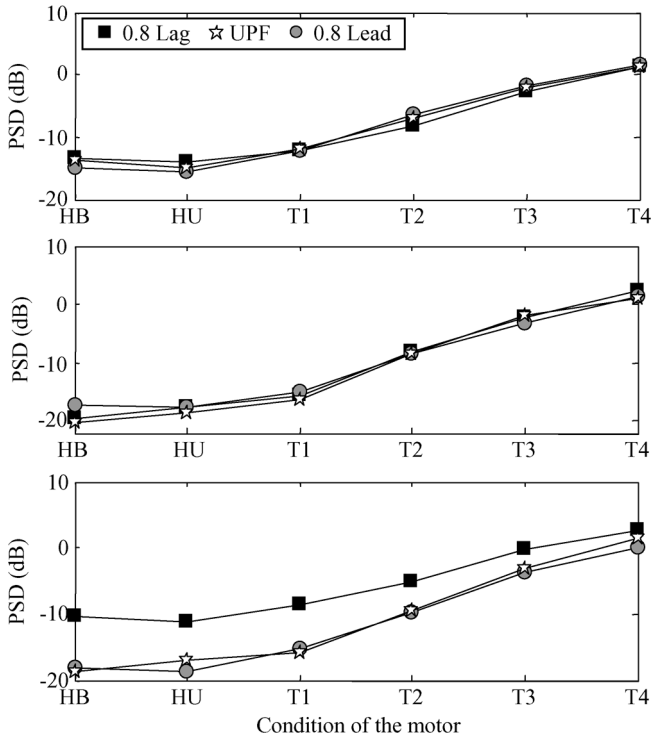

Fig. 14. 90-Hz component in the rotor search coil under (top) no-load, (middle) half-load, and (bottom) full-load (experimental).

TABLE II
HARMONICS AT NO-LOAD (0.8 LAG) CONDITION (IN DECIBELS)

	HB	HU	T1	T2	T3	T4
	Field Current					
90 Hz	-68.26 (0.76)	-68.78 (0.81)	-68.7 (0.22)	-68.71 (0.49)	-67.89 (0.44)	-68.31 (0.51)
150 Hz	-76.55 (0.49)	-76.78 (1.45)	-76.12 (0.94)	-72.17 (1.36)	-65.59 (0.56)	-61.72 (0.28)
210 Hz	-85.18 (1.46)	-82.6 (1.29)	-84.53 (0.83)	-78.96 (2.89)	-72.18 (0.29)	-68.47 (0.46)
	Rotor Search-coil					
90 Hz	-13.5 (0.09)	-13.72 (0.2)	-11.99 (0.16)	-7.46 (0.89)	-2.3 (0.49)	1.46 (0.25)
150 Hz	-23.48 (0.35)	-22.86 (0.54)	-24.74 (0.11)	-15.49 (2.09)	-5.33 (0.8)	0.55 (0.35)
210 Hz	-26.94 (0.52)	-21.42 (0.31)	-26.92 (0.18)	-21.5 (1.3)	-13.75 (0.58)	-8.78 (0.35)

In order to ensure the dependability of these harmonics, five sets of data have been collected under all conditions of the motor, healthy motor with balanced supply (HB), healthy motor with unbalanced supply (HU), and with one to four shorted turns (T1 to T4). This was repeated under no-load, half-load, and full-load conditions at three PFs [0.8-lag, 0.8-lead, and unity PF (UPF)]. The average values of the 90-, 150-, and 210-Hz components in the field current as well as in the rotor search-coil voltage are shown in Tables II–X. The corresponding sample standard deviation has been shown in brackets below each of the average value. The *low values* of the standard deviations imply *less fluctuation* of these harmonics under the given conditions of the motor. Most importantly, the 150-Hz components in the field current and the 90-Hz components in the rotor search coil *stood out prominently*.

TABLE III
HARMONICS AT NO-LOAD (0.8 LEAD) CONDITION (IN DECIBELS)

	HB	HU	T1	T2	T3	T4
	Field Current					
90 Hz	-69.21 (0.86)	-69.98 (0.74)	-68.66 (0.07)	-69.31 (0.36)	-69.09 (0.28)	-70.11 (0.29)
150 Hz	-79.07 (0.88)	-77.17 (0.71)	-82.26 (2.26)	-77.4 (0.64)	-70.31 (0.42)	-66.93 (0.28)
210 Hz	-86.14 (2.37)	-87.25 (2.27)	-86.22 (2.65)	-81.35 (0.86)	-76.16 (0.98)	-73.37 (0.59)
	Rotor Search-coil					
90 Hz	-15.06 (0.05)	-15.58 (0.06)	-12.17 (0.15)	-6.36 (0.14)	-1.72 (0.06)	1.5 (0.01)
150 Hz	-19.43 (0.2)	-21 (0.23)	-22.06 (0.33)	-13.03 (0.4)	-4.47 (0.1)	0.62 (0.02)
210 Hz	-26.77 (0.37)	-18.96 (0.24)	-26.11 (0.5)	-19.74 (0.42)	-13.19 (0.11)	-8.99 (0.08)

TABLE IV
HARMONICS AT NO-LOAD (UPF) CONDITION (IN DECIBELS)

	HB	HU	T1	T2	T3	T4
	Field Current					
90 Hz	-67.86 (0.49)	-68.7 (0.33)	-67.95 (0.29)	-68.45 (0.18)	-68.91 (0.39)	-70.14 (0.36)
150 Hz	-79.45 (1.73)	-75.68 (0.79)	-79.44 (1.26)	-77.38 (0.86)	-71.31 (0.81)	-67.17 (0.54)
210 Hz	-86.53 (1.96)	-85.34 (2.1)	-86.07 (1.96)	-81.64 (1.55)	-76.59 (1.58)	-73.65 (1.46)
	Rotor Search-coil					
90 Hz	-13.67 (0.05)	-14.96 (0.07)	-11.81 (0.08)	-6.9 (0.49)	-2.15 (0.31)	1.47 (0.15)
150 Hz	-21.16 (0.17)	-21.83 (0.23)	-22.28 (0.19)	-15.1 (1.15)	-5.64 (0.56)	0.21 (0.31)
210 Hz	-26.18 (0.22)	-20.02 (0.41)	-25.89 (0.17)	-20.98 (0.45)	-14.23 (0.49)	-9.24 (0.47)

TABLE V
HARMONICS AT HALF-LOAD (0.8 LAG) CONDITION (IN DECIBELS)

	HB	HU	T1	T2	T3	T4
	Field Current					
90 Hz	-80.28 (2.20)	-78.75 (1.31)	-77.35 (1.90)	-69.52 (0.80)	-63.53 (0.22)	-59.65 (0.28)
150 Hz	-72.46 (1.24)	-72.03 (0.91)	-75.15 (1.07)	-66.05 (0.64)	-58.25 (0.39)	-54.55 (0.28)
210 Hz	-81.45 (0.83)	-77.62 (1.66)	-79.26 (2.29)	-73.86 (1.94)	-67.14 (0.57)	-63.06 (0.29)
	Rotor Search-coil					
90 Hz	-19.45 (0.22)	-17.58 (0.03)	-15.58 (0.14)	-8.29 (0.51)	-2.46 (0.17)	2.44 (0.14)
150 Hz	-23.96 (0.28)	-24.20 (0.10)	-32.04 (0.25)	-13.88 (0.63)	-4.21 (0.19)	1.05 (0.16)
210 Hz	-35.66 (0.55)	-22.93 (0.08)	-28.33 (0.71)	-19.76 (0.31)	-12.01 (0.21)	-6.60 (0.10)

A detailed analysis, identical to the one carried out in Tables II–X, was also done for the standard field winding. The results are almost similar, suggesting that the coil structure used in winding the field does not affect the detection. One set spectral plot is shown in Fig. 15. Once again, the 90-, 150-, and 210-Hz components clearly increased with fault and showed no increase under supply unbalance.

Furthermore, in order to study if circulating currents have any effect on detectability, the stator winding of the synchronous motor was reconnected in delta with the standard field structure. The results from one set of data are shown in Table XI under one of the worst possible scenarios as far as detection sensitivity is

TABLE VI
HARMONICS AT HALF-LOAD (0.8 LEAD) CONDITION (IN DECIBELS)

	HB	HU	T1	T2	T3	T4
	Field Current					
90 Hz	-74.30 (0.28)	-75.26 (1.01)	-74.28 (0.81)	-71.35 (0.21)	-68.79 (0.54)	-66.00 (0.10)
150 Hz	-76.71 (0.61)	-77.09 (1.04)	-78.38 (1.03)	-74.34 (0.64)	-68.28 (0.36)	-63.99 (0.38)
210 Hz	-90.53 (1.79)	-82.51 (1.86)	-87.53 (1.08)	-82.15 (1.91)	-76.80 (0.27)	-72.89 (0.41)
	Rotor Search-coil					
90 Hz	-17.39 (0.01)	-17.54 (0.04)	-15.01 (0.19)	-8.71 (0.16)	-3.42 (0.39)	1.21 (0.10)
150 Hz	-25.97 (0.05)	-42.29 (0.59)	-26.32 (0.26)	-14.81 (0.40)	-6.59 (0.44)	-0.69 (0.25)
210 Hz	-26.54 (0.04)	-21.15 (0.18)	-24.72 (0.54)	-19.59 (0.45)	-13.55 (0.42)	-9.00 (0.35)

TABLE VII
HARMONICS AT HALF-LOAD (UPF) CONDITION (IN DECIBELS)

	HB	HU	T1	T2	T3	T4
	Field Current					
90 Hz	-75.68 (0.81)	-76.34 (0.88)	-74.98 (0.24)	-70.28 (0.52)	-65.09 (0.15)	-62.51 (0.71)
150 Hz	-74.94 (0.61)	-75.54 (0.89)	-76.41 (0.71)	-70.11 (0.25)	-62.53 (0.21)	-58.60 (0.56)
210 Hz	-85.88 (0.97)	-81.64 (1.25)	-81.69 (2.14)	-78.31 (1.44)	-71.22 (0.51)	-67.06 (0.21)
	Rotor Search-coil					
90 Hz	-20.10 (0.11)	-18.57 (0.09)	-16.03 (0.46)	-8.42 (0.08)	-2.21 (0.10)	1.85 (0.46)
150 Hz	-25.85 (0.29)	-28.87 (0.33)	-28.91 (0.30)	-13.93 (0.15)	-4.77 (0.21)	0.44 (0.55)
210 Hz	-30.90 (0.44)	-23.04 (0.21)	-25.40 (0.16)	-18.63 (0.13)	-12.13 (0.36)	-7.22 (0.21)

TABLE VIII
HARMONICS AT FULL-LOAD (0.8 LAG) CONDITION (IN DECIBELS)

	HB	HU	T1	T2	T3	T4
	Field Current					
90 Hz	-70.6 (0.53)	-71.48 (0.79)	-71.26 (0.43)	-73.83 (0.57)	71.18 (0.58)	-67.11 (0.62)
150 Hz	-79.67 (2.28)	-81.68 (1.65)	-77.19 (1.97)	-71.18 (1.14)	65.66 (0.40)	-62.63 (0.42)
210 Hz	-81.28 (2.12)	-77.43 (1.13)	-78.51 (0.75)	-77.32 (1.41)	75.78 (0.61)	-75.08 (0.69)
	Rotor Search-coil					
90 Hz	-10.29 (0.12)	-11.22 (0.07)	-8.69 (0.05)	-5.01 (0.03)	-0.21 (0.08)	2.66 (0.04)
150 Hz	-24.45 (0.12)	-27.52 (0.21)	-36.2 (0.32)	-17.56 (0.15)	-7.69 (0.2)	-3.23 (0.11)
210 Hz	-24.95 (0.3)	-21.58 (0.47)	-21.51 (0.15)	-16.12 (0.1)	-1.67 (0.42)	-9.39 (0.23)

concerned. The trend looks almost similar to Table III that was also obtained under identical operating conditions.

A close look at the detailed tabulated results clearly reveals that the magnitudes of these harmonics are dependent on the operating point of the machine. A probable reason may be explained by looking closely at Table I. For example, the 90-Hz component can be caused by both $k = 1$ and 5. Similarly, the 150-Hz component can be caused by both $k = 3$ and 7. Due to the variations in the load and PF, the space distribution of these components may change, resulting in a variation of detection. Other factors such as, saturation, other time harmonics, and eccentricity-related low-frequency components might also

TABLE IX
HARMONICS AT FULL-LOAD (0.8 LEAD) CONDITION (IN DECIBELS)

	HB	HU	T1	T2	T3	T4
	Field Current					
90 Hz	-81.05 (1.7)	-82.8 (1.21)	-78.55 (0.59)	-78.19 (0.75)	-75.87 (0.19)	-73.88 (0.34)
150 Hz	-85.27 (1.51)	-83.98 (1.56)	-84.45 (1.31)	-83.38 (0.94)	-80.06 (1.01)	-76.24 (0.66)
210 Hz	-89.32 (1.25)	-84.47 (1.44)	-89.37 (0.93)	-86.58 (0.76)	-85.88 (1.03)	-83.84 (1.13)
	Rotor Search-coil					
90 Hz	-18.1 (0.05)	-18.63 (0.05)	-15.15 (0.05)	-9.58 (0.11)	-3.72 (0.12)	0.37 (0.23)
150 Hz	-26.16 (0.27)	-28.7 (0.51)	-24.35 (0.22)	-17.45 (0.11)	-9.68 (0.16)	-4.55 (0.59)
210 Hz	-25.66 (0.18)	-20.68 (0.19)	-23.41 (0.18)	-19.25 (0.07)	-14.34 (0.24)	-10.67 (0.37)

TABLE X
HARMONICS AT FULL-LOAD (UPF) CONDITION (IN DECIBELS)

	HB	HU	T1	T2	T3	T4
	Field Current					
90 Hz	-85.16 (2.19)	-89.15 (0.46)	-84.72 (2.35)	-85.84 (1.04)	-74.83 (0.58)	-69.66 (0.45)
150 Hz	-80.7 (1.01)	-84.82 (1.37)	-80.01 (1.28)	-75.67 (0.9)	-70.66 (0.47)	-66.86 (0.48)
210 Hz	-85.7 (2.6)	-83.34 (1.86)	-84.31 (1.86)	-81.6 (0.81)	-78.56 (1.31)	-75.26 (0.59)
	Rotor Search-coil					
90 Hz	-18.63 (0.03)	-16.98 (0.25)	-15.7 (0.16)	-9.54 (0.16)	-2.99 (0.25)	1.45 (0.12)
150 Hz	-28.75 (0.04)	-34.98 (0.67)	-31.6 (0.29)	-17.83 (0.26)	-8.13 (0.36)	-2.44 (0.25)
210 Hz	-27.18 (0.16)	-22.39 (0.41)	-24.72 (0.42)	-18.83 (0.46)	-12.87 (0.48)	-8.73 (0.34)

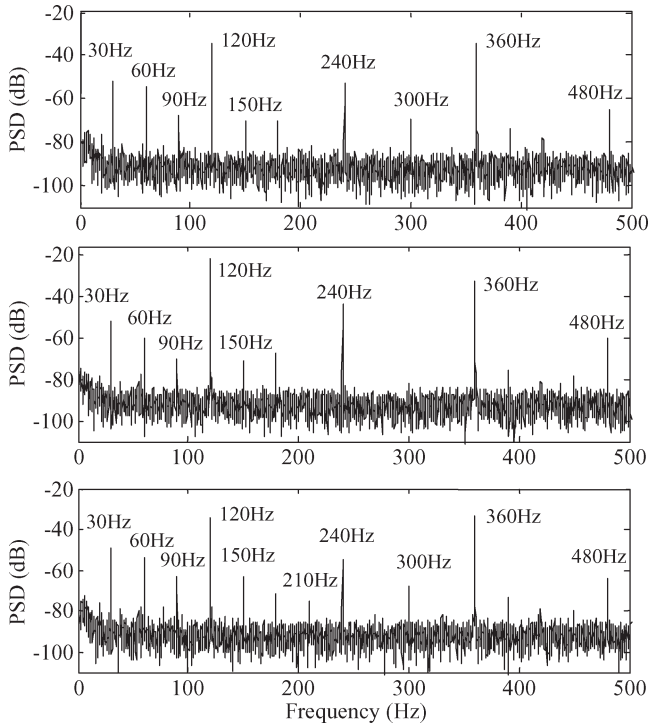

Fig. 15. Experimental PSD of field current under full-load 0.8 lagging PF condition (top) with balanced supply, (middle) with unbalanced supply, and (bottom) four-turn fault for a standard field winding.

TABLE XI
HARMONICS AT NO-LOAD (0.8 LEAD, DELTA) CONDITION (IN DECIBELS)

	HB	HU	T1	T2	T3	T4
	Field Current					
90 Hz	-64.51	-65.08	-64.00	-63.75	-63.12	-63.47
150 Hz	-77.39	-75.80	-78.69	-82.29	-80.46	-73.93
270 Hz	-83.24	-87.32	-83.00	-78.59	-79.68	-77.48
	Rotor Search-coil					
90 Hz	-13.65	-13.60	-11.05	-5.27	-1.18	2.15
150 Hz	-13.00	-14.40	-17.00	-12.63	-3.72	1.78
270 Hz	-27.35	-26.73	-27.80	-23.81	-20.54	-16.10

TABLE XII
HARMONIC COMPONENTS IN FIELD CURRENT DUE TO 120-HZ TIME HARMONIC IN STATOR VOLTAGE AND CURRENT

k	1	2	3	4	5	6	7	8	9	10
Freq. (Hz)	90	60	30	0	30	60	90	120	150	180
	150	180	210	240	270	300	330	360	390	420

TABLE XIII
HARMONIC COMPONENTS IN FIELD CURRENT DUE TO 180-HZ TIME HARMONIC IN STATOR VOLTAGE AND CURRENT

k	1	2	3	4	5	6	7	8	9	10
Freq. (Hz)	150	120	90	60	30	0	30	60	90	120
	210	240	270	300	330	360	390	420	450	480

cause changes in them. Tables similar to Table I can evaluate the influence of other time harmonics. Tables XII and XIII show the influence of the 120- and 180-Hz time harmonics [predominant ones in supply voltage, as seen in Fig. 9 (top)], respectively, on the field harmonics. A possible way to circumvent this problem is to have a lookup table describing the best harmonic to be selected in the field current or the rotor search-coil voltage under a given operating condition.

Furthermore, the method using the search coil has been tested with a commercial inverter in the open-loop voltage/frequency mode and was found to be capable of detecting interturn faults unambiguously at both 60 and 30 Hz [18].

Overall, it can be said with certainty that the pursuit of similar harmonic components to detect stator faults, particularly in the rotor search coil of any salient-pole synchronous machine, holds distinct promise.

VIII. CONCLUSION

New results to detect stator interturn faults in a salient-pole synchronous motor have been obtained by analyzing the field current of the machine. The scheme is capable of detecting the less severe state of the fault unambiguously, particularly with supply unbalance and time harmonics. The internal asymmetry of the machine that has adversely affected the earlier fault diagnosis results has, for the first time, been shown as an advantage. A detailed theoretical proof for the induction of various frequency components has been furnished. A simulation study was carried out on four different cases involving two types of field windings. Detailed experimental results have been presented, showing the influence of the load and PF of the machine on the diagnosis results. The 150-Hz component in the field current can be a very *good indicator* of fault and is able to detect up to three-turn faults unambiguously. Further research will be directed toward improving the level of sensitivity in field-current harmonics. Analyzing the voltage induced in the rotor search coil also validates the diagnosis results. The 90-Hz component in the rotor search coil appears to be an *extremely promising indicator of even* a *one-turn fault without any correction factor*. The low values of standard deviations indicate *less fluctuation* of these harmonics at any given condition and, hence, imply more dependability. The scheme can be very easily implemented to ensure the rapid tripping of the faulty machine at a cheaper cost since only one signal has to be analyzed. The proposed method can be used for both salient-pole and round-rotor synchronous machines.

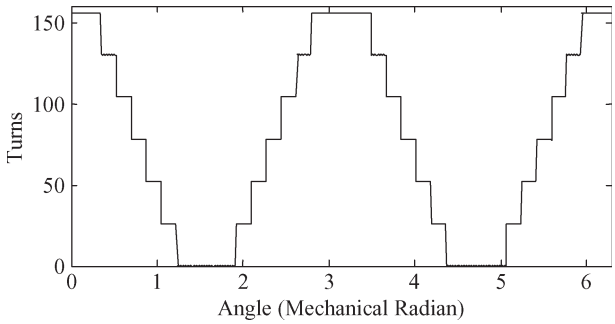

Fig. 16. Turn functions of the healthy stator phase-a.

APPENDIX

The modeling of an interturn fault in the stator winding can be carried out using WFA and MWFA as follows. The turn function of a *healthy* stator phase-a winding has been shown in Fig. 16. Its Fourier expansion can be given as

$$n_A(\phi) = a_{os} + \sum_{m=1,3,5,\ldots}^{\infty} a_{ms}\cos(pm\phi)$$
$$a_{os} = \frac{3N}{2} \qquad N = 26$$
$$a_{ms} = \frac{2N}{\pi m}\sin\left(\frac{\pi m}{3}\right)\left\{1 + 2\cos\left(\frac{\pi m}{9}\right)\right\}. \quad \text{(A1)}$$

The stator of SM has a double-layer lap winding with 26 conductors per slot per phase (312 turns/phase). Results have been obtained with one to four consecutive shorted turns in stator slots 27–33 of phase-a. With four shorted turns, the turn function of a *shorted part* of the stator phase-a winding has been shown in Fig. 17. Its Fourier expansion can be given as

$$n_{Af}(\phi) = a_{osf} + \sum_{c=1,2,3,\ldots}^{\infty} a_{csf}\cos\left\{c\left(\phi + \frac{\pi}{18}\right)\right\}$$
$$a_{osf} = \frac{N_s}{6}; \quad a_{csf} = \frac{2N_s}{\pi c}\left\{\sin\left(\frac{\pi c}{6}\right)\right\}. \quad \text{(A2)}$$

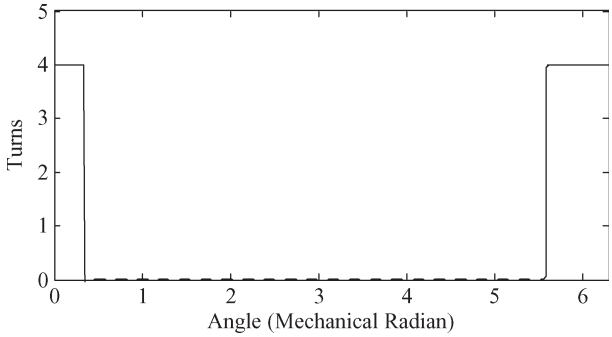

Fig. 17. Turn functions of the faulty part of stator phase-a.

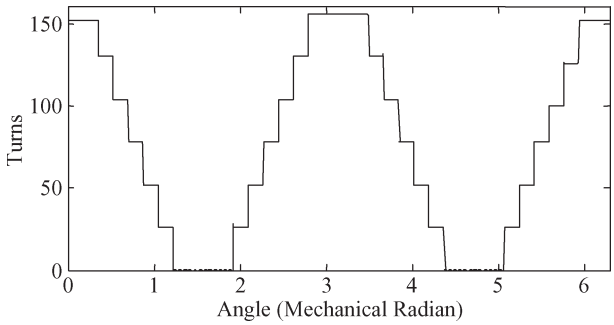

Fig. 18. Turn functions of the healthy part of stator phase-a.

The turn function of the *healthy part* of the stator phase-a winding can be expressed as

$$n_{Ah}(\phi) = n_A(\phi) - n_{Af}(\phi). \tag{A3}$$

The turn function of the *healthy part* of the stator phase-a winding has been shown in Fig. 18. Using these turn functions, various magnetizing and mutual inductances of the machine can be computed using WFA and MWFA [13]–[16]. Using the computed inductances, the dynamic model of the SM with interturn fault can be developed.

REFERENCES

[1] G. B. Kliman, W. J. Premerlani, R. A. Koegl, and D. Hoeweler, "A new approach to on-line turn fault detection in ac motors," in *Conf. Rec. IEEE IAS Annu. Meeting*, Oct. 1996, vol. 1, pp. 687–693.

[2] D. W. Auckland, I. E. D. Pickup, R. Shuttleworth, Y. T. Wu, and C. Zhou, "Novel approach to alternator field winding interturn fault detection," *Proc. Inst. Elect. Eng.—Gener. Transm. Distrib.*, vol. 142, no. 2, pp. 97–102, Mar. 1995.

[3] R. J. Streifel, R. J. Marks, II, M. A. El-Sharkawi, and I. Kerszenbaum, "Detection of shorted-turns in the field winding of turbine-generator rotors using novelty detectors—Development and field test," *IEEE Trans. Energy Convers.*, vol. 11, no. 2, pp. 312–317, Jun. 1996.

[4] J. S. Hsu and J. Stein, "Shaft signals of salient-pole synchronous machines for eccentricity and shorted-field-coil detections," *IEEE Trans. Energy Convers.*, vol. 9, no. 3, pp. 572–578, Sep. 1994.

[5] X. H. Wang, Y. G. Sun, B. Ouyang, W. J. Wang, Z. Q. Zhu, and D. Howe, "Transient behavior of salient-pole synchronous machines with internal stator winding faults," *Proc. Inst. Elect. Eng.—Electr. Power Appl.*, vol. 149, no. 2, pp. 143–151, Mar. 2002.

[6] J. Penman and H. Jiang, "The detection of stator and rotor winding short circuits in synchronous generators by analysing excitation current harmonics," in *Proc. Int. Conf. Opportunities Adv. Int. Electr. Power Gener.*, Mar. 1996, pp. 137–142.

[7] J. Sottile, F. C. Trutt, and A. W. Leedy, "Condition monitoring of brushless three-phase synchronous generators with stator windings or rotor circuit deterioration," in *Conf. Rec. IEEE IAS Annu. Meeting*, Sep./Oct. 2001, vol. 3, pp. 1587–1594.

[8] S. Wan, H. Li, Y. Li, and Y. Wang, "The diagnosis method of generator rotor winding inter-turn short circuit fault based on excitation current harmonics," in *Proc. Int. Conf. IEEE-PEDS*, Nov. 2003, vol. 2, pp. 1669–1673.

[9] P. Neti and S. Nandi, "An improved strategy to detect stator inter-turn faults in synchronous reluctance machines using both negative sequence quantities and stored magnetic energy after supply disconnection," in *Conf. Rec. IEEE IAS Annu. Meeting*, New Orleans, LA, Sep. 2007, pp. 2234–2241.

[10] J. R. Cameron, W. T. Thomson, and A. B. Dow, "Vibration and current monitoring for detecting airgap eccentricity in large induction motors," *Proc. Inst. Elect. Eng.*, vol. 33, no. 3, pt. B, pp. 155–163, May 1986.

[11] G. Kron, *Equivalent Circuits of Electric Machinery*. New York: Wiley, 1951.

[12] G. B. Kliman, R. A. Koegl, J. Stein, R. D. Endicott, and M. W. Madden, "Noninvasive detection of broken bars in operating induction motors," *IEEE Trans. Energy Convers.*, vol. 3, no. 4, pp. 873–879, Dec. 1988.

[13] X. Luo, Y. Liao, H. A. Toliyat, A. El-Antably, and T. A. Lipo, "Multiple coupled circuit modeling of induction machines," *IEEE Trans. Ind. Appl.*, vol. 31, no. 2, pp. 311–318, Mar./Apr. 1995.

[14] H. A. Toliyat and T. A. Lipo, "Transient analysis of cage induction machines under stator, rotor bar and end ring faults," *IEEE Trans. Energy Convers.*, vol. 10, no. 2, pp. 241–247, Jun. 1995.

[15] H. A. Toliyat, M. S. Arefeen, and A. G. Parlos, "A method for dynamic simulation of air-gap eccentricity in induction machines," *IEEE Trans. Ind. Appl.*, vol. 32, no. 4, pp. 910–918, Jul./Aug. 1996.

[16] N. A. Al-Nuaim and H. A. Toliyat, "A novel method for modeling dynamic air-gap eccentricity in synchronous machines based on modified winding function theory," *IEEE Trans. Energy Convers.*, vol. 13, no. 2, pp. 156–162, Jun. 1998.

[17] S. Nandi and H. A. Toliyat, "Novel frequency-domain-based technique to detect stator interturn faults in induction machines using stator-induced voltages after switch-off," *IEEE Trans. Ind. Appl.*, vol. 38, no. 1, pp. 101–109, Jan./Feb. 2002.

[18] P. Neti, "Stator fault analysis of synchronous machines," Ph.D. dissertation, Univ. Victoria, Victoria, BC, Canada, 2007.

Prabhakar Neti (S'04–M'07) received the B.Tech. degree in electrical engineering from Sri Venkateswara University, Tirupati, India, in 1994, the M.Tech. degree in electrical engineering from Jawaharlal Nehru Technological University, Hyderabad, India, in 1996, and the Ph.D. degree in electrical and computer engineering from the University of Victoria, Victoria, BC, Canada, in 2007.

From 1996 to 2002, he was a Faculty Member at different engineering colleges in India. From May 2007 to April 2008, he was a Postdoctoral Fellow with the Department of Electrical and Computer Engineering, University of Manitoba, Winnipeg, MB, Canada. He is currently with the Electric Machines and Drives Laboratory, Electronics and Energy Conversion, General Electric Global Research Center, Niskayuna, NY. His research interests are mainly in the area of modeling and fault diagnosis of electric machines and drives.

Subhasis Nandi (S'97–M'00–SM'06) received the B.E. degree in electrical engineering from Jadavpur University, Calcutta, India, in 1985, the M.E. degree in electrical engineering from the Indian Institute of Science, Bangalore, India, in 1988, and the Ph.D. degree in electrical engineering from Texas A&M University, College Station, in 2000.

He is currently an Associate Professor in the Department of Electrical and Computer Engineering, University of Victoria, Victoria, BC, Canada. Between 1988 and 1996, he was with TVS Electronics and the Central Power Research Institute, Bangalore, India, working in the areas of power electronics and drives. His main research interests are power electronics and drives and the analysis and design of electrical machines, with special emphasis on fault diagnosis.